A Segmented Deployable Primary Mirror for Earth Observation from a CubeSat Platform

Noah Schwartz, David Pearson, Stephen Todd, Andy Vick, David Lunney, Donald MacLeod
UK Astronomy Technology Centre
Blackford Hill, Edinburgh, EH9 3HJ, UK; +44 131 6688 256
noah.schwartz@stfc.ac.uk

ABSTRACT

The aperture size is the primary limitation on the resolving power of an optical system, so deployable optical systems provide a means of improving the spatial sampling that can be provided within a fixed launch volume. The UK ATC has been developing a CubeSat sized deployable optical system that can co-phase its primary aperture based on image metrics derived from the science scene. Discussed are the telescope optical design and tolerances, the mechanical design of the primary optic, together with the deployment and actuation systems, and the image metrics that are used to co-phase the system. A breadboard optical system has been designed, manufactured and tested and the results are presented and used to derive operational feasibility and next steps towards a in orbit demonstrator.

INTRODUCTION

Described is the development of a breadboard demonstrator of a deployable optical telescope designed to fit within a 3U CubeSat but with the potential to be realised at a range of sizes. The system provides a demonstration platform for the deployment and articulation of the main mirror segments and a test platform for the development of the control algorithms, based on relatively simple image metrics, which provide the alignment and co-phasing control of the opto-mechanics.

Deployable optical systems for large space missions have considerable heritage[1] and continue to be at the forefront of space optics technology[2]. Small satellites have broadly the same need for deployable optics; to maximise the angular resolution and light gathering power for a launch volume. As well as EO imaging and spectro-imaging, deployable optics are of interest to communications[3] and LIDAR systems[4]. Several developments are on-going; the FalconSat-7 team[5] are developing a deployable diffractive optical system with benign tolerances to misalignment, SDL[6] have been developing a highly integrated and accurate petal telescope mechanism and TU-Delft[7] have been studying a three mirror deployable telescope design.

Motivation

The optical aperture of an imaging system imposes a physical limit on its angular resolution. In the case of an Earth Observation (EO) imager at a fixed distance, this angular resolution directly relates to a maximum spatial resolution of the ground, and the aperture size is determined by the physical dimensions of the satellite. EO applications are demanding ever greater spatial resolutions so, in order to maximise the optical aperture for a given satellite size and mass, the use of a deployable optical telescope system has been proposed. At high spatial resolutions, when the effective ground speed necessitates a short integration time, or in high dispersion systems, the increased collecting power of the larger aperture has additional benefits in signal-to-noise.

Technical objectives

This work is part of a series of ongoing studies into deployable optical telescopes and, at this stage, the technical objectives were;

1) To develop an optical design that provided suitable image quality for a relatively wide FoV Earth Imaging system at visible wavelengths, that could fit into the 3U CubeSat volume (folded) and could be deployed and actuated for co-phasing.
2) To develop and test the deployment and actuation systems for the main mirror segments.
3) To test a number of image metrics using representative scenes and estimate the co-phasing accuracy and final image sharpness that a co-phasing algorithm can produce.

OPTICAL DESIGN

Assumptions and requirements

The primary mirror is assumed to consist of four square panels, each 90mm square. Once deployed, they form the arrangement shown in Figure 1. This gives a maximum baseline of approximately 300mm, which defines the diffraction limited resolution of the system as 0.46 arcsec at 550nm.
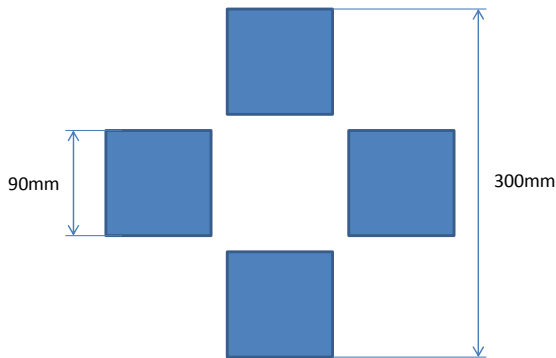

Figure 1: The configuration of the four segments of the primary mirror

In order to define the optical parameters of the system we assumed a detector pixel size of 13 μm. When combined with the spatial resolution required on the ground, this determines the required focal length of the optical system. If we want to fully sample the diffraction limited image (0.23 arcsec per pixel) then this implies a focal length of 11700 mm (focal ratio of f/39). At an altitude of 350 km this plate scale corresponds to 0.39 m/pixel on the ground, allowing objects of around 0.8 m to be resolved (2 pixels). A CCD array 2k pixels wide would give a complete swath width of 0.8 km.

The telescope must be very compact in order to allow relatively simple deployment from a 3U CubeSat. For this study we have constrained the separation of primary to secondary mirror to a maximum of 200mm, and the separation from secondary mirror to detector to a maximum of 250mm.

Design overview

The design shown in Figure 2 produces the required f/40 beam at the detector. Different plate scales could be produced by changing the lens elements with a minor re-optimization of the telescope mirrors. The telescope is a Cassegrain telescope consisting of two mirrors with non-zero conic constants. M1 is very close to being a parabola, and consists of the four deployable segments.
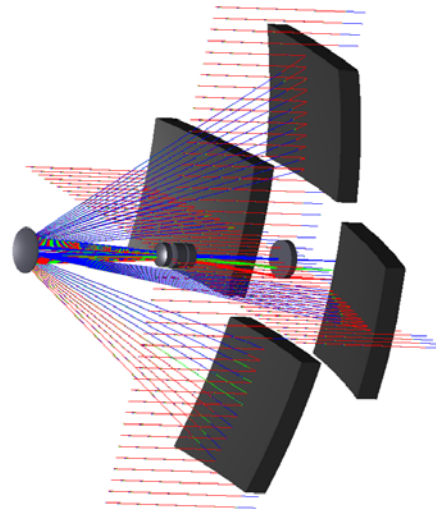

Figure 2: The optical design of the telescope system with the four lens corrector system

Without the lenses the telescope operates at around f/6.3. The lenses increase the focal length of the telescope while also correcting off-axis aberrations and field curvature across the visible wavelength band. All lens surfaces are spherical, and the lens materials are standard commercially available glasses. This system gives excellent diffraction limited performance across the field of view and across the visible wavelength band. The resulting point spread function is shown in Figure 3.
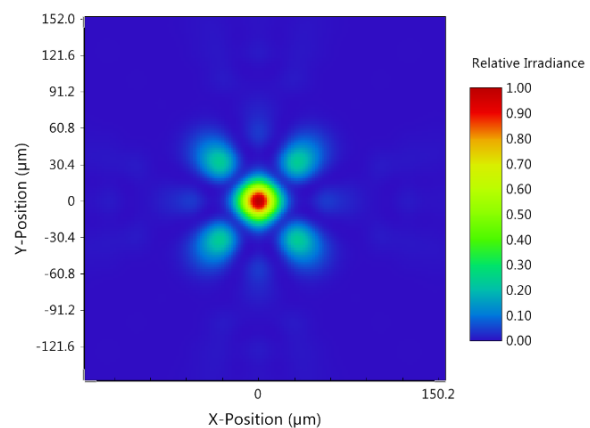

Figure 3: The point spread function generated by the telescope.

Sensitivity to misalignment

Analysis shows that the system is extremely sensitive to small misalignments of the segments. This is to be expected when attempting to form a single optical surface with diffraction limited performance.

The sensitivity to tilt and focus allows us to estimate the resolution of movement required in these axes to achieve co-phasing of the segments. A Monte-Carlo analysis in Zemax OpticStudio showed that over 90% of cases are diffraction limited (wavefront error better than $\lambda/14$) when tolerances of $\pm 4 \times 10^{-5}$ degrees for the two tilt axes and ± 30nm in focus are used.

There is a very high sensitivity to decenter of the segments – even a 1 µm decenter has a significant effect. This is a result of the very fast focal ratio of the primary mirror (f/0.75). This misalignment can be compensated to some degree by adjusting the tilt and focus of the segment, but a significant residual wavefront error remains. As a result, the decenter of the segments needs to be correct to within around 10 µm. This places a tight requirement on the initial alignment of the system and on the repeatability of positioning defined by the hinges of the deployment mechanism.

Increasing the radius of curvature of the primary mirror reduces the sensitivity to decenter of the segments. This would require an increase in the separation between M1 and M2, making the telescope longer and hence requiring a more complex deployment mechanism for M2. Such a change would do nothing to relax the resolution requirements for the tilt and focus adjustments of the segments. These sensitivities are independent of the optical design of the telescope, and simply reflect the deviation of the surface of the segment relative to the nominal optical surface.

A summary of the mechanical requirements for co-phasing this optical system to achieve diffraction-limited performance are provided in Table 1.

Table 1: Mechanical requirements for co-phasing

DOF	Adjustment resolution	Adjustment stroke	Deployment repeatability
Tip	$\pm \lambda/14$ ($\pm$ 45 nm)	1 mm	$\pm$ 10 µm
Tilt	$\pm \lambda/14$ ($\pm$ 45 nm)	1 mm	$\pm$ 10 µm
Piston	$\pm \lambda/14$ ($\pm$ 45 nm)	1 mm	$\pm$ 10 µm

MECHANICAL DESIGN

The prototype mirror system has been designed for operation within a generic space environment (i.e. operation within a low-gravity vacuum). The aluminum construction of the base, mechanisms and mirrors means that the optical geometry will remain invariant in uniform steady state thermal environments. Transient thermal effects have not been considered at this stage.

The optical surface is diamond-cut on to an aluminum substrate. The four machined surfaces form a parabola with their optical axis passing through the center of the assembly. This does not exactly match the prescription which would be required as part of a complete telescope assembly (see above), but has been chosen for this demonstration to allow optical testing using a collimated beam and a return sphere without the need for additional optics.

The mechanism designs are based on the requirements provided in Table 1, and all non-actuated degrees of freedom of the mirror (i.e. radial and tangential positions) are machined to an accuracy of $\pm$ 10 µm.

Mirror adjustment

The design of the mirror is a direct consequence of the packaging, adjustment and deployment strategies. Figure 4 shows an overview of the mirror design. The mirror has two integral v-grooves that locate its axis of revolution. These v-grooves were also used as the tooling fixtures for to ensure the diamond-cut surface is precisely aligned to its assembled position in the CubeSat base. A third tooling fixture (a pad on the rear of the mirror) was required to ensure the mirror did not deform during diamond turning.
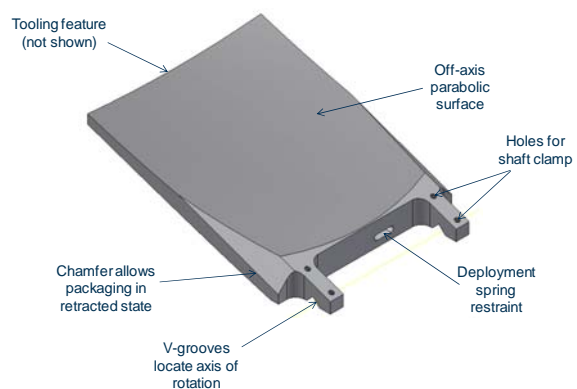

Figure 4: Mirror design overview

Each mirror is clamped to a solid steel shaft that rotates with the mirror. The shaft is mounted into two v-grooves that are integrally machined into parallel flexures. Figure 5 shows this arrangement. The shaft is

steel because it is required to be very stiff and also the steel-aluminum interface at the v-groove has better friction properties than an all-aluminum interface (a reduced susceptibility to galling).

The white arrows in Figure 5 show the direction of flexure. These two flexures provide the tilt adjustment of the mirror. The use of parallel flexures means that the hinge v-groove does not rotate when displaced vertically. The concept is effectively a 'floating hinge' design, actuated by a force from beneath. The shaft is held into the floating hinge by means of a small cap made from Vespel SP3. This material was chosen for its low friction coefficient when in contact with steel. No oil- or grease-based lubricants have been used in the design.
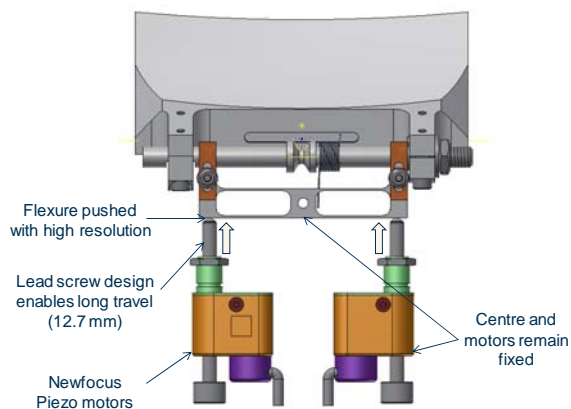

Figure 5: Mirror flexure and tilt motor assembly

Two NewFocus 8354 piezo motor drives are placed underneath the flexures and define the position of the floating hinge. These motors were chosen for this purpose because they:

- Are unable to be back-driven
- Are static when powered down
- Provide a relatively high actuation force (13 N)
- Have a long stroke length (12.7 mm)
- Are vacuum compatible
- Have a positioning resolution < 30 nm
- Are easy to integrate
- Have compact and low power drive electronics

The operating principle of the chosen motors uses a pair of small piezoceramic pads that asynchronously expand and contract to turn a lead screw. They have no encoder and are run open loop. This is acceptable for this application because the confirmation of the mirror position will be done using the co-phasing algorithms, as described in the next section.

The drive electronics for the NewFocus motors are low power and compact. The prototype system uses a Newport 8742 4-channel driver, which is easily configurable for lab use, but the final system will require a component similar to the single channel PCB mountable product (Newport 8712) to be compatible with the CubeSat volume and power constraints.

The mirror tilt is provided by third motor and flexure combination onto which an arm from the mirror rests. This arm is held on the flexure by the force of two torsion springs on the mirror shaft. Figure 6 shows this arrangement. Contact between the mirror arm and the third flexure is only made after deployment. The motor, flexure and arm positions are carefully chosen to avoid clashes with the other three mirror arms that also require a deployment arc.

The combination of three motors on each mirror can be used to create the tip, tilt or piston motion of each mirror segment. The four mirrors, twelve flexures and twelve motors are assembled as four tessellated 'L' shapes when viewed in planform. This is achieved by mounting all the mirrors onto a central aluminum substrate into which the eight shaft flexures are integrally machined. This complicated component is necessary to guarantee that the tangential and radial alignment of the four mirrors could be manufactured to meet the 10 μm requirement without the need for shimming or adjustment. The shafts are located tangentially (i.e. axially) by a small steel flexure held by a v-groove also on the central substrate, again manufactured to within ±10 μm.
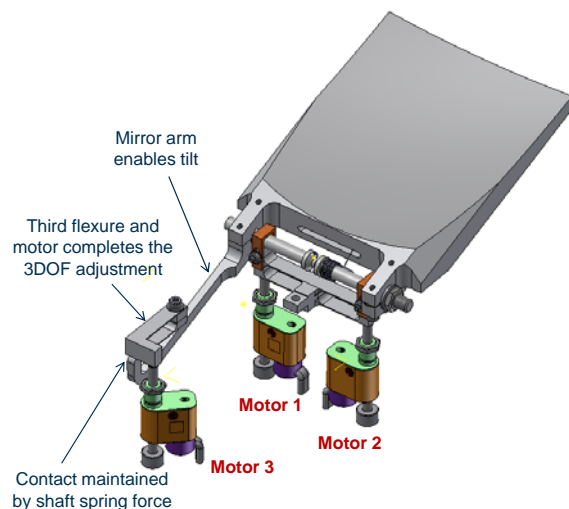

Figure 6: Tip motor arrangement

Figure 7 and Figure 8 show the final arrangement of the CubeSat design in the folded and deployed states,

respectively. The mirrors were chosen to be solid aluminum for ease of manufacture and to demonstrate feasibility of the concept in the prototype design. For a space-ready instrument the mirror design would be optimized for low mass.

The final volume of the folded system is 100 x 100 x 150 mm, which is 1.5 CubeSat units. This leaves 1.5 units for housekeeping, communications, control, processing and data storage electronics.
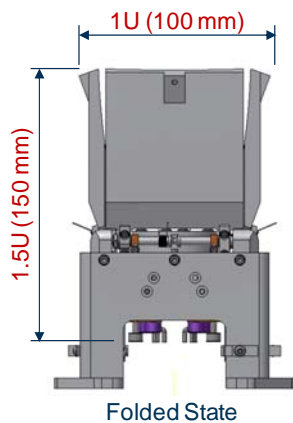

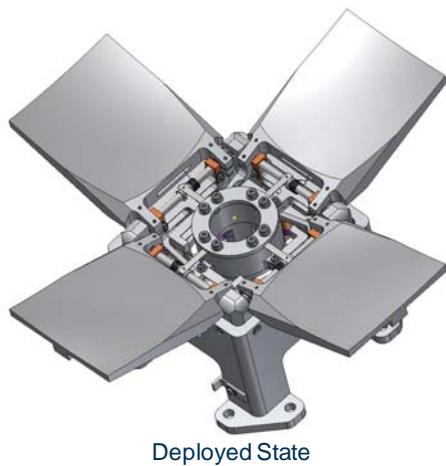**Figure 7: Mirror assembly in folded state**

Figure 8 Mirror assembly in deployed state

Mirror deployment

The mirror is deployed by means of a captive torsion spring. The motion of the spring is damped to provide a steady rate of deployment until the mirror arm contacts the tilt flexure. The segments can be deployed individually or in unison and the total deployment time is approximately 10-15 seconds.

Test data

The testing of the alignment resolution was performed using a Zygo DynaFiz interferometer in double pass with a return sphere.

A typical image from the interferometer is shown in Figure 10. The measurements were taken with approximately 5-10 fringes across the mirror. The interferometer measurement used a mask diameter of 84 mm and so covered most of the mirror surface. A small flat mirror was mounted to the rear tooling point of the parabolic mirror (visible at the bottom of Figure 9) to aid alignment.
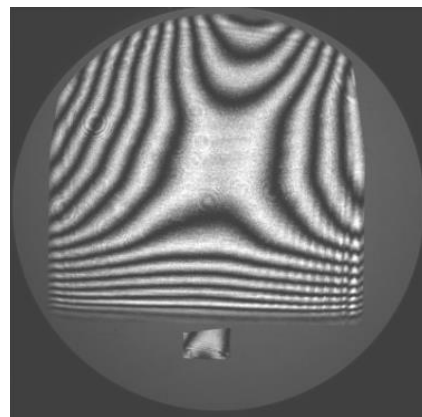

Figure 9: An interferometric image of the mirror

To test the deployment, the mirror was folded up and then released back into the path of the interferometer. A tip-tilt measurement was then taken using a second-order Zernike fit. The difference between the measurement after each deployment and the initial position of the mirror provides the relative positional error in tip and tilt. Figure 10 shows the tip-tilt deployment errors for the first 13 deployments. The blue circles indicate the measurement uncertainty. The maximum error is approximately 8 fringes (2.5 μm at a half-wavelength of 316 nm) but more typically within 4 fringes.

To test the alignment resolution of the mirrors, the three piezo motors were individually moved in blocks of 10 steps and the fringe pattern was measured after each move using a Zernike fit. Figure 11 shows the change in value of Zernike coefficients Z2, Z3 and Z4 (tilt, tip and piston, respectively) when motor 1 is moved from zero motor steps, up to sixty steps, then back to zero.

It can be seen that motor 1 produces a combined tip/tilt motion of the mirror, as expected for its location at the base of the mirror arm (see Figure 5). The mirror does not return precisely to its starting point, which indicates hysteresis or backlash within the system occurring at

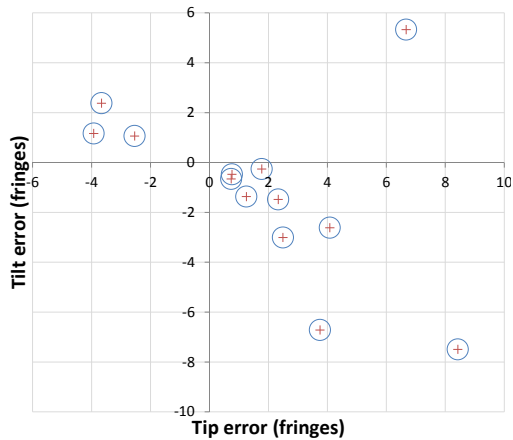the point where the direction of the motor movement is reversed.
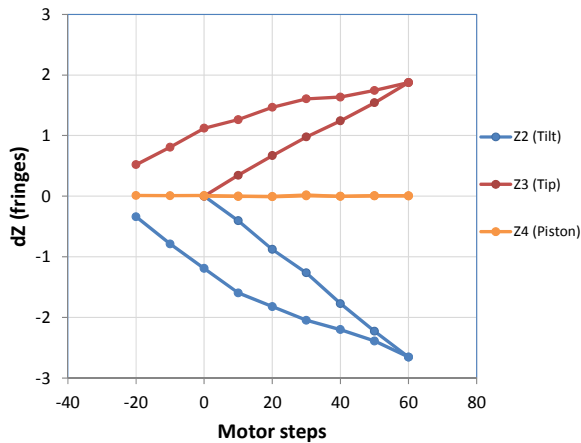

Figure 10: Deployment accuracy

Figure 11: Motor 1 adjustment

The cause of this nonlinearity is not clear and could either be a property of the motor or effects due to flexure and friction within the mirror mechanism assembly. However, it is observed that the initial movement of the mirror from step zero to sixty was approximately linear. The mirror tilted (Z2) 2.5 fringes in 60 motor steps, which means it moved λ/24 per step and therefore meets the design requirement in Table 1. Single-step measurements could not be measured because they were within the measurement noise of the interferometer.

The levels of hysteresis or backlash were large compared to the positioning resolution of the motor. From Figure 11 it is estimated that the motor would have had to move 90-100 steps to return the mirror from its displaced position at 60 steps back to its start point. These distances are representative of what the mirror would be required to move as part of the co-

phasing routine, and so requiring 30 extra steps is a concern. However, the step count has no direct bearing on the adjustments required by the algorithm, but the nonlinearity of the movement will need to be taken into account in the software. Further tests are needed to fully characterize this behavior.

The trends observed in the movement of motor 1 also applied to motors 2 and motor 3. Namely, a linear motion followed by a nonlinear return back to the start position. The linear positional resolution of motor 2 was measured as λ/40 and for motor 3 as λ/50, due to the longer distances between the points of actuation and the mirror center of rotation.

OPTICAL METROLOGY

Having demonstrated the performance of the opto-mechanical hardware, the use of using image sharpness as a mean to align and co-phase (i.e. creating a synthetic single optical surface limited by diffraction) the 4 petals of the CubeSat was then investigated. Consistent with the mechanical prototype, it was assumed that each mirror segment could be manipulated in three degrees of freedom (i.e. piston, tip and tilt) and that each mirror segment could be deployed sequentially and its position optimized in turn.

Image formation

The diffractive point spread function (PSF) was generated using OpticStudio and then imported into Matlab (see Figure 12). The Matlab script took control of the model parameters, such as segment position, in order to optimize image quality. The ground scene image was then convolved with the calculated PSF to generate the final aberrated images: *image = scene * PSF* (where * represents the convolution). This method assumed a PSF invariant by translation. The variation of the PSF across the field was investigated separately and was shown to be negligible both in the case of the nominal system and in the presence of misalignments.
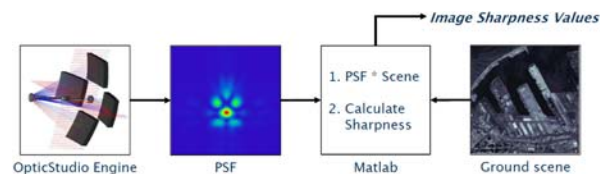

Figure 12: Simulation strategy.

To test the system, a number of ground scenes that are representative of different terrains (e.g. forest, city, desert…), were selected. These images had a ground sampling distance of 0.5 m. The effects of aberrations on the metrics are symmetrical and only half the range is studied. For tip and tilt, the range of aberration studied is 0 to 7.2 arcsec and for piston 0 to 2 μm

Impact of segments on image

The unconventional pupil shape used (i.e. 4 separate petals), leads to a distinct point spread function and modulation transfer function (MTF). Figure 13 shows typical PSFs and MTFs for a circular, square and for the present design with a 4-petal aperture.
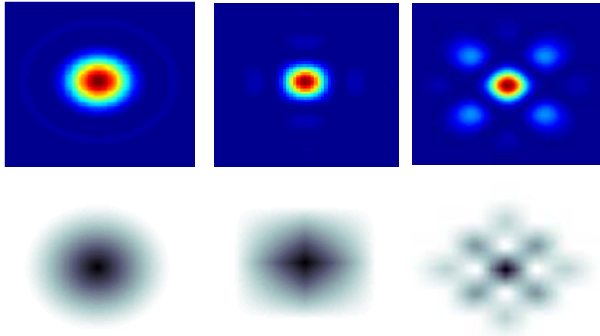

Figure 13: Comparison of circular (left), square (centre) and 4-petal aperture (left) PSFs (top) and MTF (bottom).

The shape of the PSF will naturally have an impact on the final image. Figure 14 shows this effect for a circular aperture of 9 cm (i.e. the maximal aperture size of a CubeSat without deployment), the 4-petal design and a full 30 cm circular aperture (i.e. the maximal dimension of the 4-petal CubeSat without any gaps between segments).
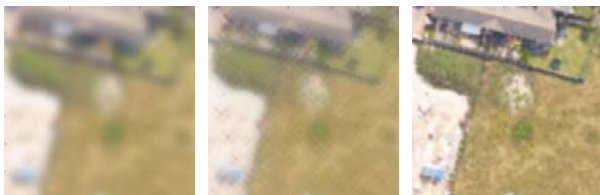

Figure 14: Image comparison - circular aperture with diameter of 9 cm (left) and 30 cm (right) and 4-petal design (center).

The shape of the 4-petal PSF (with high side lobes; approx. 25% of central lobe) clearly has an impact on the final image (i.e. visible 'waffle' features). However, the overall resolution is significantly better than for a 9 cm circular aperture and the effects 'waffle' features could potentially be mitigated by deconvolution.

What is not visible from Figure 14 however, is the improvement in signal-to-noise. The signal is multiplied by a factor approximately 5 by increasing the aperture area from a 9 cm circular aperture to the 4-petals design. A full 30 cm circular aperture would give another 2 fold increase in signal above the 4-petal system.

Co-phasing mirror segments

In order to retrieve the full diffraction limited capability of the 300 mm diameter aperture, the position of the 4 petals needs to be known and adjusted to form a synthetic single optical surface. Being on a CubeSat platform significantly constrains the choice of metrology systems capable of measuring the position of a segmented primary mirror in all 3 degrees of freedom (i.e. piston, tip and tilt); the available volume is very limited and so is the electric and computing power. Candidate metrology systems need to have a large aberration capture range (approx. 10 μm), a high precision measurement of segment position (approx. 10-20 nm) and a sampling bandwidth limited to a few Hz. Several technologies are available, namely: direct wavefront sensing (using for example a Shack-Hartmann), phase diversity analysis, direct measurements using displacement sensors, or inspection of the image sharpness. The first two would require addition hardware which is not compatible with a CubeSat platform, and no suitable displacement sensors could be identified. Therefore the inspection of image sharpness was selected as the most suitable approach.

Image sharpness metrics

It is important that the image sharpness metrics have certain characteristics to enable a co-phasing algorithm to be developed:

- Maximum: The metric needs to have a maximum (or a minimum) for the aberration-free images.
- Monotonicity: Ideally, the metric should increase or decrease monotonically away from the extremum.
- Range: The sharpness metric should have sufficient variation over a large range of aberrations.
- Sensitivity: The sharpness metric should be sensitive to small misalignments.
- Noise: Signal-to-noise ratio should have limited impact on metric.

Several metrics have been investigated, namely: square intensity, standard deviation, edge detection filter (Sobel), Haar wavelength, and frequency methods. The frequency methods work by applying a high-frequency and/or low-frequency pass filter to the image (see Figure 15). The filters can either be circular or square, and can either be apodised (i.e. gradual transition from non-filtered frequencies to filtered frequency) or top-hat (i.e. direct transition between non-filtered frequencies and filtered frequencies).
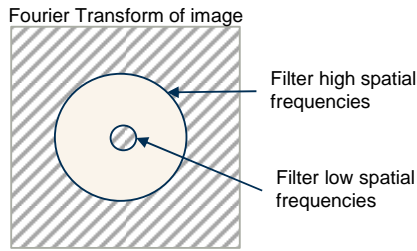
Figure 15: Image sharpness – Illustration of the frequency methods.

Detailed performance comparisons of each of these metrics have shown that the frequency methods offer the best potential for co-phasing mirror petal segments, with respect to the five characteristics identified. Simulations of the co-phasing process were then undertaken for each of the degrees of freedom.

Piston
Figure 16 presents the normalised image sharpness (frequency method) for the deployment of the third segment. It was assumed that the first two segments were perfectly aligned, and perfect tip-tilt positioning of the segment under consideration. The different coloured lines represent different scenes. It can be seen that the global decrease is accompanied by an oscillation in the metric value, i.e. the decrease is not monotonic and is subject to local minima. This due to the 2π modulus of the wavefront. This means that any chosen optimization routine needs to reject local minima in order to find a bounded global maximum.
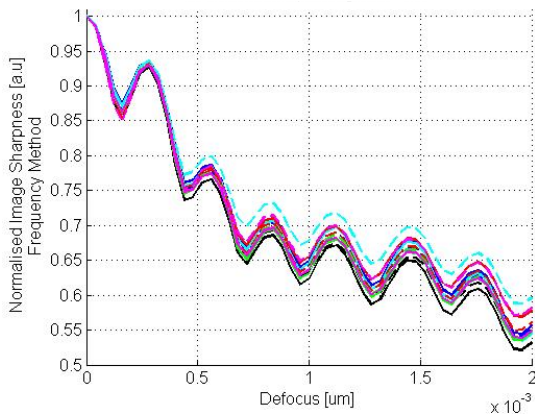

Figure 16: Normalized image sharpness as a function of piston assuming the first 2 petals are perfectly aligned.

Tip & Tilt
Figure 17 presents the normalised image sharpness (frequency method) for the deployment of the fourth segment. Similar to the piston study, a perfect alignment of the first three segments and perfect piston and tilt about Y of the segment under consideration is

assumed. The different coloured lines represent different scenes. In contrast to the piston metric, the tip and tilt metrics show a monotonic decrease over the mirror angles investigated, but the response is of lower amplitude than the piston metric. Nevertheless, the monotonicity greatly simplifies any potential optimization algorithms and shows promise for the tip/tilt co-phasing of these segments.
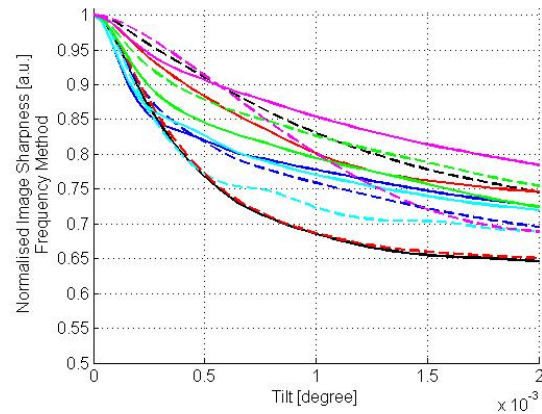

Figure 17: Normalized image sharpness as a function of the tilt about X assuming the first 3 petals are perfectly aligned.

Discussion

It was found that the best overall metrics for optimizing tip, tilt and piston were obtained by selecting the spatial frequencies content of the image. Selecting the range of frequencies used in the metrics can mitigate their sensitivity to image content. However, finding a metric that is completely insensitive to image content is not possible. Measuring piston produces damped oscillations that will naturally make the optimization process a challenge. Measuring tip and tilt however is more straightforward (monotonic decrease).

The sensitivity of the image sharpness metrics to change in mirror segment angle is compatible with positioning capabilities of the prototype mechanism. For example, Figure 10 shows that the deployment accuracy is typically better than 8 fringes (or 2.5μm at a half-wavelength of 316 nm) over an interferometer mask of diameter 84 mm. This equates to an initial angular error of the segments of 1.7×10^{-3} degrees in tip and tilt, which is within the range of the metric shown in Figure 17. Similarly, the adjustment resolution shown in Figure 11 of at least 24 motor steps per fringe is sufficient to enable a viable optimization algorithm to be developed in tilt. The piston adjustment may require higher adjustment resolutions to cope with the metric oscillations seen in Figure 16, and this remains an open topic for further investigation.

CONCLUSIONS AND FURTHER WORK

A concept for a deployable primary mirror in a CubeSat has been presented. A mechanical prototype of this concept was developed and it is shown that the deployment and alignment positional tolerances required for the co-phasing of the mirror segments can be achieved. The prototype is packaged within 1.5U CubeSat volume and uses space-compatible hardware.

The use of image sharpness metrics has been shown to be a viable method of co-phasing the four mirror segments. This was demonstrated using simulations. The metric works particularly well for tip and tilt positioning, but in piston the 2π modulation of the wavefront poses additional challenges.

The next steps in this project are to test the co-phasing algorithms on the prototype mechanisms and to measure the optical performance under lab conditions.

ACKNOWLEDGEMENTS

REFERENCES

1. Lightsey, Paul A., et al., "James Webb Space Telescope: large deployable cryogenic telescope in space", Optical Engineering, Volume 51, Issue 1, Jan. 2012.

2. Bolcar, Matthew R., et al., "Technology development for the Advanced Technology Large Aperture Space Telescope (ATLAST) as a candidate large UV-Optical-Infrared (LUVOIR) surveyor", Proc. SPIE, Volume 9602, Sept. 2015.

3. Bedington, R., et al., " Deploying quantum light sources on nanosatellites II: lessons and perspectives on CubeSat spacecraft ", Proc. SPIE, Volume 9648, Oct. 2015.

4. Mazzinghi, P., et al., "Deployable, lightweight, and large aperture spaceborne telescope for lidar-based earth observations", Proc. SPIE, Volume 6750, Oct 2007.

5. Dearborn, M. E., et al., "FalconSat-7: Imaging the Sun with a Low Cost Deployable Membrane Telescope from a 3U CubeSat", American Geophysical Union, Fall Meeting 2012, AGU Dec. 2012.

6. Champagne, J., et al., "CubeSat Image Resolution Capabilities with Deployable Optics and Current Imaging Technology", 28th Annual AIAA/USU Conference on Small Satellites, Utah State University, 2014.

7. Dolkens, D., "A Deployable Telescope for Sub-Meter Resolutions from MicroSatellite Platforms", Masters Thesis, TU Delft (Delft Technical University) Feb 2015.